

ROLE OF Y³⁺ IONS ON THE STRUCTURAL AND DIELECTRIC PROPERTIES OF Ni-Zn-Cr FERRITES SYNTHESIZED BY CO-PRECIPITATION METHOD

N. AMIN^a, M. IMRAN ARSHAD^a, M. U. ISLAM^c, A. ALI^a, K. MAHMOOD^a
G. MURTAZA^c, M. AHMAD^b, G. MUSTAFA^{c*}

^aDepartment of Physics, Government College University, Faisalabd, 38000
Pakistan

^bDepartment of Physics, COMSATS Institute of Information Technology,
Lahore54000, Pakistan

^cDepartment of Physics, BahauddinZakariya University Multan 60800, Pakistan

In this study spinel ferrites Ni_{0.5}Zn_{0.5}Cr_{0.04}Y_xFe_{1.96-x}O₄ (x = 0.0, 0.02, 0.04 and 0.06) were synthesized using the co-precipitation method by varying the concentration of Yttrium. X-ray diffraction (XRD) and Fourier transform infrared (FTIR) analysis confirm the formation of spinel ferrites structure. The average particle size estimated by Scherrer formula found to be in the range 30.3-106 nm with cubic shape. Energy Dispersive Spectroscopy (EDS) measurement was in close agreement with the stoichiometry of the reactant solutions. UV-Vis-NIR spectroscopy evidenced intermediate energy levels within the band gap of the prepared ferrites system. Dielectric measurements showed that the inverse relation of permittivity of these ferrites with frequency that follows the Maxwell Wagner Model. The substituted samples exhibited very low dielectric constant and low loss tangent in the frequency range 1 MHz to 3GHz. AC conductivity increased with the increase in frequency and decreased with the increase of yttrium concentration. Such characteristics of these materials may be suitable for potential applications such as switching and microwave devices.

(Received March 18, 2016; Accepted May 26, 2016)

Keywords: Spinel ferrites; co-precipitation; X-ray diffraction; AC conductivity.

1. Introduction

Electrical and optical properties of Ferrites are strong of chemical composition, cation distribution, sintering temperature and time, additive amount of the cations and method of preparation. The soft magnetic behavior in ferrites is caused by the exchange interaction among the cations on the polyhedral sites. The 4f orbitals of rare earth cations is key to the electrical and magnetic properties of ferrites [1-2]. Generally, 4f orbitals are tailored by controlling the type and the amount of different substitutes of cations [3-4] distribution in ferrites at tetrahedral and octahedral sites. It is well known that high resistivity of nickel ferrites with proper doping of divalent ions (Zn²⁺, Co²⁺, and Mn²⁺), trivalent ions (Al³⁺ and Cr³⁺) and rare earth (RE) ions (Nd³⁺, Dy³⁺, Y³⁺, Pr³⁺, and Sm³⁺), have acquired special attention due to a large functional diversity [5-10] in modern telecommunications and electronic devices [11-12]. It is well documented in the literature that the resistivity generally increases with decreasing grain size and high resistivity make these ferrites suitable for high-frequency applications where low eddy current losses are required. Ferrites substituted with rare earth ions have an improved microwave behavior compared to non-substituted materials [9] which minimize the electromagnetic reflections with high dc resistivity and complex permeability. Various methods have been adopted to synthesize rare earth metals doped ferrites including co-precipitation, sol-gel, hydrothermal, micro-emulsion and solid state reaction [13-16]. Ahmad et al., [17] reported that the substitution of rare earth metals

*Corresponding author: ghulammustafabzu@gmail.com

in ferrite system have influence on doping process and lower the Curie temperature [18]. The substitution of yttrium in ferrites system decreases the crystallite size that results in favorable structural properties [19]. The aim of present work is to explore the effect of Y^{3+} substitution on the structural and dielectric properties of $Ni_{0.5}Zn_{0.5}Cr_{0.04}Y_xFe_{1.96-x}O_4$ ferrites system synthesized by co-precipitation technique. Chief aim of present investigation is to prepare samples for the use of microwave devices.

2. Materials and Methods

2.1. Samples preparation and equipments

The chemical reagents including $Ni(NO_3)_2 \cdot 6H_2O$, $Zn(NO_3)_2 \cdot 6H_2O$, $Cr(NO_3)_3 \cdot 6H_2O$ (Aldrich, 98%), $Fe(NO_3)_3 \cdot 9H_2O$ (Aldrich, 99%), Y_2O_3 , citric acid and ethanol were used to prepare the ferrites in the composition: $Ni_{0.5}Zn_{0.5}Cr_{0.04}Y_xFe_{1.96-x}O_4$ ($x = 0.0, 0.02, 0.04, \text{ and } 0.06$) by co-precipitation method. These chemicals were weighed in the above mentioned stoichiometric proportion and dissolved in distilled water for 30 min in an ultrasonic cleaner. First yttrium oxide (Y_2O_3) was dissolved in HNO_3 by heating up to $60^\circ C$. During the heating, solution was stirred continuously with a magnetic stirrer. After this ammonia solution (i.e. NH_4OH), was added until to attain the pH of 10. An intermediate precipitate was observed in the solution, which was stirred for 1 hour to maintain the homogeneity. The solution containing precipitates was placed in water bath at $85^\circ C$ for 1hr under the ambient atmosphere. The precipitates were filtered by a filter paper (No.41) with the help of a suction flask operating on the vacuum pump. Finally, these precipitates were washed with distilled water to remove impurities. The co-precipitated powder was dried at $110^\circ C$ for 12 hours in an oven. The dried precipitates were mixed homogeneously in an agate mortar and pestle for 30 min. The obtained powder was pelletized under the load of $61N/cm^2$ for 3min by Paul-Otto Weber Hydraulic Press. The pellets (6mm x2 mm) and the powder were sintered at $900^\circ C$ for 8h in a programmable furnace. The surfaces of all the samples were polished in order to remove any oxide layer during the process of sintering. A bulk density was measured on the basis of weight and dimensions of the samples. The above synthesis process can be expressed by the following chemical reaction and also presented in the flow diagram in Fig. 1.

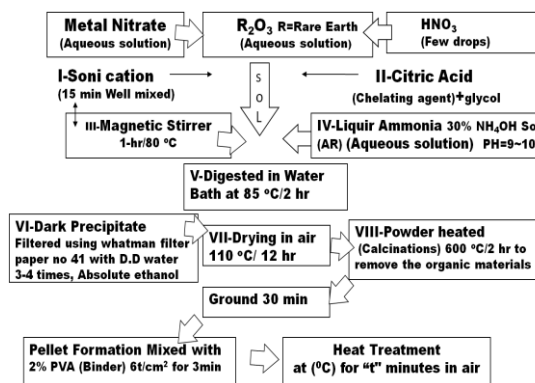
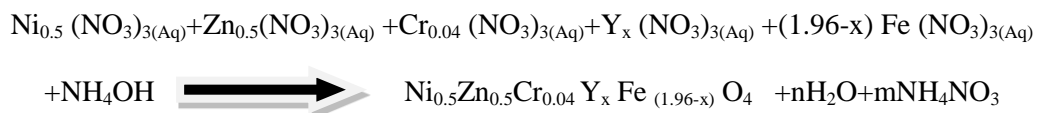


Fig. 1 Flow Diagram of Experimental Procedure

The X-ray diffraction (XRD) patterns were obtained at room temperature by powder samples in an Xpert Pro PANalytical diffractometer with $Cu-K\alpha$ radiation ($\lambda = 1.5405 \text{ \AA}$) at 40 kV and 30 mA. Intensity data were collected by the step counting method (with a scanning speed $0.05^\circ/s$) in the 2θ range from 25° - 65° . In addition, the Fourier transform infrared spectra (FT-IR)

were measured in the frequency range of 400-4000 cm^{-1} using Jasco-310 spectrometer. Surface morphology and microstructure of the samples were studied by JSM-6490 JEOL scanning electron microscope (SEM). The elemental composition was determined by energy dispersive peak of the representative sample using energy dispersive X-ray spectroscopy (EDXS, Model JFC-1500 JEOL). Normal incidence absorbance of the synthesized samples was recorded at room temperature over wave length range of (200-1100 nm) using Perkin El-mer UV/Vis/NIR Lambda spectrophotometer. The complex dielectric function measurements were performed with HP4291A material impedance analyzer in conjunction with a HP4194 Impedance Analyzer, which jointly cover the region of 1MHz to 3GHz. For this purpose the electrodes were deposited by silver paste on both sides of a sample and dried out at 200 °C for 10 °C/ min.

2.2 Calculations

Structural properties were determined from the XRD measurements and lattice constant 'a' unit cell volume, crystallite size 'D', bulk density, X-ray density, porosity and lattice strain (ϵ_{rms}) were calculated using the following formulae [20-21].

$$a = \frac{\lambda}{2\sin\theta} \sqrt{h^2 + k^2 + l^2} \quad (1)$$

The spinel cubic unit cell volume was calculated (where $a = b = c$ and $\alpha = \beta = \gamma = 90^\circ$)

$$V_{\text{cell}} = a^3 \quad (2)$$

The analysis of the crystallite size (D) nm, of the synthesised ferrites samples which have single phase was determined by using the Scherer's equations.

$$D = \frac{k\lambda}{B_{(hkl)}\cos\theta} \quad (3)$$

Where k is the shape coefficient (value between 0.9 and 1.0), λ is the X-ray wavelength, B is the full width at half maximum (FWHM) of each Phase and θ is the Bragg's diffraction angle. The bulk density was determined by the following equation.

$$\rho_{\text{bulk}} = \frac{m}{V} \quad (4)$$

Where 'm' is the mass and 'V' ($=2\pi r^2 h$, where r is the radius and h is the height/thickness of pellet) is the volume of the pellet. The X-ray density was determined according to the relation:

$$\rho_{\text{X-ray}} = \frac{Z M}{N_A V} \quad (5)$$

Where, V is the unit cell volume, Z represents 8 molecules per unit cell of the spinel structure, N_A is the Avogadro's number (6.02×10^{23} g/mol) and M is the molecular weight of the sample. The porosity (P) in % of the samples was calculated from bulk density and X-ray density values using the expression.

$$P \% = 1 - \frac{\rho_{\text{bulk}}}{\rho_{\text{X-ray}}} \quad (6)$$

The lattice strain (ϵ_{rms}) of the samples was calculated by the relations:

$$B_G^2 = 8\pi(\tan^2 \theta)(\epsilon_{rms}^2) \quad (7)$$

Where B_G is the integral width (defined as the peak area divided by peak height) of peak in radian. Dielectric constant ϵ' , dielectric loss $\tan \delta$, and AC conductivity was calculated from the measured data. Ferrite samples prepared in the capacitor form can be considered electrically equivalent to a capacitance C_p in parallel with a resistance R_p . These values (C_p and R_p) were measured directly using the impedance analysis and important electrical parameters were calculated using the following equations [22-23].

$$\epsilon' = \frac{C_0}{C_p} \quad \text{where } C_0 = \frac{A\epsilon_0}{d} \quad (8)$$

$$\tan \delta = \frac{1}{\omega C_p R_p} \quad (9)$$

$$\sigma_{ac} = \omega \epsilon_0 \epsilon' \tan \delta \quad (10)$$

where C_0 is the sample capacitance in vacuum which depends on the electrode spacing (d) and the electrode area (A), ω is the angular frequency of the applied field and ϵ_0 is the permittivity in vacuum equal to 8.85×10^{-12} F/cm.

3. Results and Discussions

3.1. Crystal Structure Analysis

Fig.2 shows the X-ray diffraction patterns of $\text{Ni}_{0.5}\text{Zn}_{0.5}\text{Cr}_{0.04}\text{Y}_x\text{Fe}_{1.96-x}\text{O}_4$ ($x = 0.0, 0.02, 0.04$ and 0.06) ferrite system synthesized through co-precipitation technique and annealed at 900°C for 6 h. Diffraction peaks corresponding to the planes (220), (311), (222), (400), (422), (511/333), (440) confirmed the synthesis of spinel ferrite structure. Table I enlists the various structural properties calculated using equations 1–7. It was found that the lattice constant and unit cell volume increased with the increase in Y^{3+} contents. For $x = 0.02$, the replacement of the smaller Fe^{3+} ions (0.64\AA) with larger Y^{3+} ions (0.95\AA) with already presence of Cr^{3+} (0.63\AA) causes dilation of the host spinel lattice that causes a decrease in the lattice constant $a = 8.354\text{\AA}$ as compared to pure sample. Furthermore, it was observed that for $x = 0.04$ and $x = 0.06$ (which equalize the Cr^{3+} ion and Y^{3+} ion at B site) lattice constant increased.

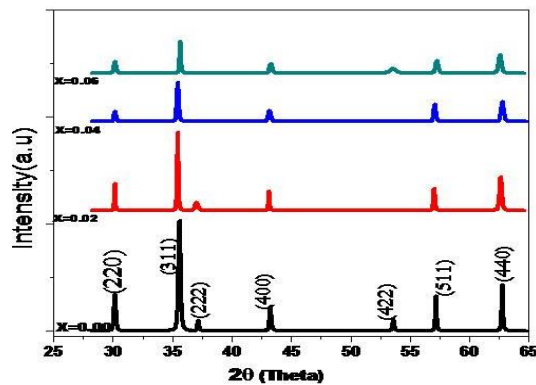


Fig. 2 X-ray Diffraction of Ni-Zn-Cr-Y-Fe spinel ferrites ($x=0.00-0.06$) annealed at 900°C for 6h

The crystallite size was 106 nm for pure ($x=0.00$) and for the Yttrium doped samples it was in the range of 30.3-38.6 nm. The values of bulk density were found in range of $4.2-4.7\text{ g/cm}^3$ which may be due to inhibition of grain growth by the substitution of Y^{3+} into the spinel lattice. The X-ray density increased by enhancing the Y^{3+} substitution which was due to the larger molar mass of yttrium (88.905 amu) as compared to iron (55.845 amu). The effect of metal cation

substitution on the porosity was in the range of 12.3–21.3 % .The linearity trends in calculated lattice strain was found to vary from 1.1×10^3 - 3.7×10^3 .

Table I: Lattice constant, volume of the unit cell, crystallite size (nm), bulk density (d_m), X-ray density (d_x), porosity (% P) and lattice strain (ϵ_{rms}) at yttrium substitution of Ni-Zn-Cr ferrites

Parameters	X=0.00	X=0.02	X=0.04	X=0.06
Lattice constant, a (Å)	8.380	8.354	8.390	8.430
Volume of the unit cell (Å ³)	588.48	583.01	590.59	599.08
Crystallite size D(nm)	106	38.6	30.3	30.3
d_m (g/cm ³)	4.22	4.37	4.69	4.70
d_x (g/cm ³)	5.36	5.28	5.37	5.46
Porosity (%P)	21.3	17.2	12.6	13.9
Lattice strain (ϵ_{rms}) $\times 10^3$	1.1	3.7	3.7	2.9

3.2 FTIR spectra studies

Fig. 3 shows the Fourier transform infrared spectra here the presence of two absorption bands below 1000cm^{-1} was a common feature observed in all ferrites [25]. Further investigation showed two absorption bands (ν_1) and (ν_2) that were attributed to the intrinsic vibrations of the tetrahedral and octahedral group complexes respectively. The tetrahedral (ν_1) and octahedral (ν_2) bands occur in the range $530\text{-}540\text{ cm}^{-1}$ (ν_1) and $400\text{--}418\text{ cm}^{-1}$ (ν_2) in samples with yttrium concentration of $x=0.04$ and 0.06 . The octahedral band ν_2 seemed to be widened with Y^{3+} concentration; this may be due to the statistical distribution of the Fe^{3+} ions on tetrahedral and octahedral sites [27-28]. The change in the peak intensity of the spectra has been noticed with increasing Y^{3+} contents and was related to the change of dipole moment with the inter-nuclear distance [29] that represented the contribution of the ionic bond Fe–O in the lattice. It was assumed that the observed increase in the peak intensity could be attributed to the perturbation occurring in Fe–O bonds by the substitution of yttrium ions from $x=0.04$ to 0.06 .

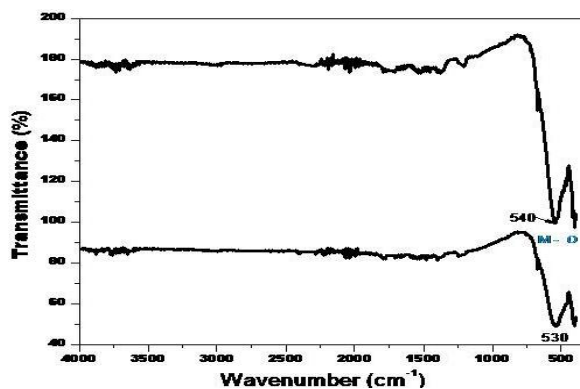


Fig. 3 FTIR spectra of Ni-Zn-Cr-Y-Fe spinel ferrites ($x=0.04, 0.06$)

3.3 Morphology and Elemental analysis

Fig.4 shows the SEM micrographs of representative samples $x = 0.04$ and $x = 0.06$. The micrographs of the sample $x = 0.04$ exhibited the homogeneous grain size distribution with spherical shapes. The agglomerates were observed in the investigated ferrite samples, the appearance of these agglomerates may be attributed to the sintering process as a result of chemical reaction. Magnetic forces or even relatively weak Vander Waals bonds might be responsible to hold these agglomerates together [30]. The mobility of grain boundaries can be of significance in the grain growth therefore presence of Y^{+3} ions near or at the grain boundaries confined the grain boundary movement subsequently the grain size decreased with increasing Y^{+3} substitution [31].

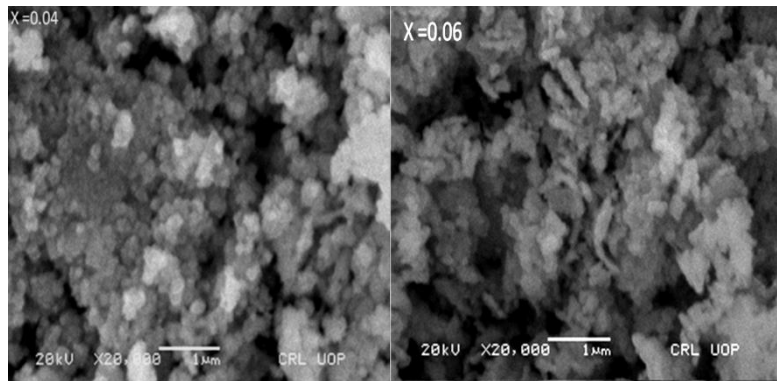


Fig. 4 SEM Micrographs for Ni-Zn-Cr-Y-Fe spinel ferrite at $x=0.04$ and 0.06

Fig. 5 shows the energy dispersive X-ray spectra of the representative composition of the investigated sample. The analysis of these spectra indicates that mixed oxides have fully undergone the chemical reaction to form the required oxide materials.

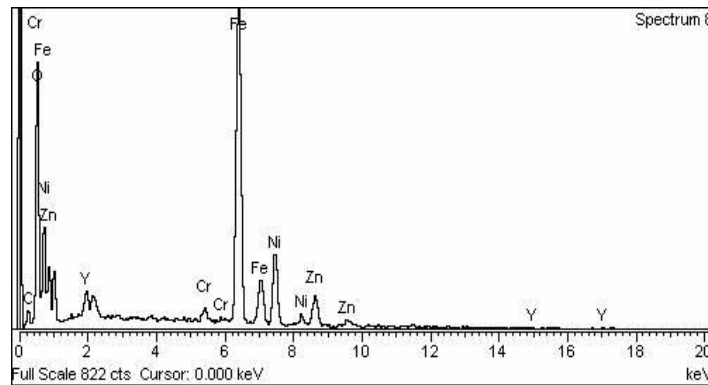


Fig. 5 EDX Spectrum for Ni-Zn-Cr-Y-Fe spinel ferrite at $x=0.04$

3.4 Optical Properties:

Fig.6 illustrates the UV/Vis spectra of the Y^{+3} substituted Ni-Zn-Cr ferrites, the absorbance decreased as the doping of Y^{+3} increase and the wavelength lies most prominently in UV region wavelength 200-380 nm approximately. An intense peak at 470.6 nm pointed toward the excitation of π electrons in the spinel cubic structure. Another absorption edge appeared at 1076 nm representing the presence of oxygen-containing groups linked with a cubic structure. An additional peak was noted at 1076 nm and it could be due to the presence of ZnO, Cr_2O_3 and Fe_3O_4 oxides. Moreover, in the spectrum, absorption peak at 230 nm was red shifted to 268 nm due to the reduction of Y^{+3} substituted Ni-Zn-Cr ferrites.

3.4.1 Band gap

The optical band gap and the absorption coefficient of the synthesized ferrites was calculated by Eq. (11) [32]:

$$\alpha h\nu = A(h\nu - E_g)^n \quad (11)$$

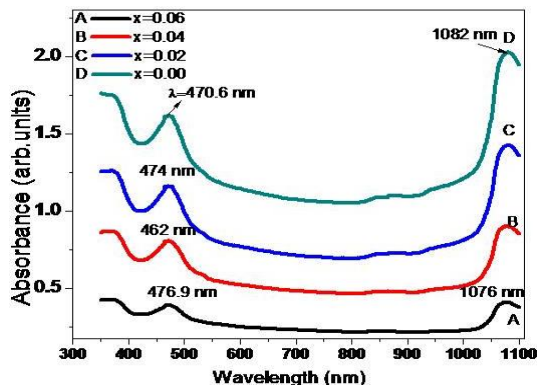


Fig.6 Ultraviolet-visible absorption spectra of the Y^{+3} -substituted Ni-Zn-Cr-ferrites at $x=0.00, 0.02, 0.04$ and 0.06

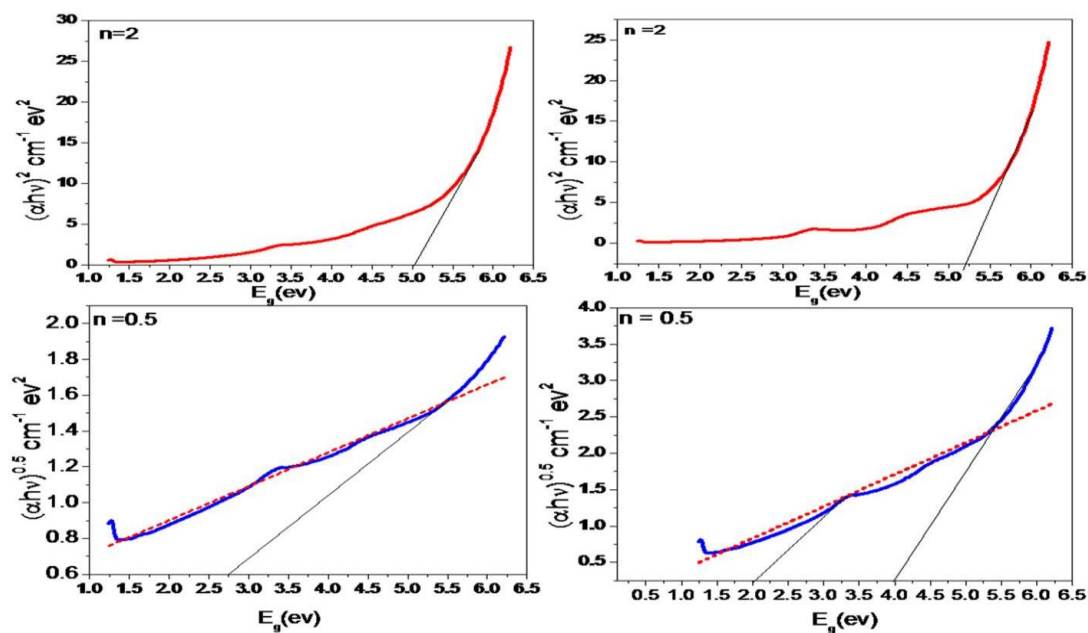


Fig.7 (a-d) Plots $(\alpha h\nu)^n$ Vs Photon energy (eV) where $n=0.5$ and 2

where ‘ α ’ is the linear absorption coefficient of the material, $h\nu$ is the photon energy ‘ A ’ is a proportionality constant, E_{gap} is the optical band gap energy and ‘ n ’ is a constant associated with different kinds of electronic transitions ($n = 1/2$ for a direct allowed and $n = 2$ for an indirect allowed). It was observed that by increasing the concentration of the Y^{+3} ions in the ferrites band gap increases. From Fig. 7 (a-d) illustrated that the direct band gap of Y^{+3} doped ferrites was lower than the indirect band gap.

3.5 Dielectric properties

3.5.1. Frequency dependence of dielectric constant

Fig. 8 shows the real (ϵ') part of dielectric permittivity in the frequency range 1 MHz to 3GHz measured at room temperature. Dielectric constant was high at low frequency and decreases

with the frequency [33]. Koops [34] suggested two factors about dielectric dispersion: (i) Electron hopping between Fe²⁺ and Fe³⁺ ions and (ii) Space charge polarization due to the presence of an inhomogeneous dielectric structure.

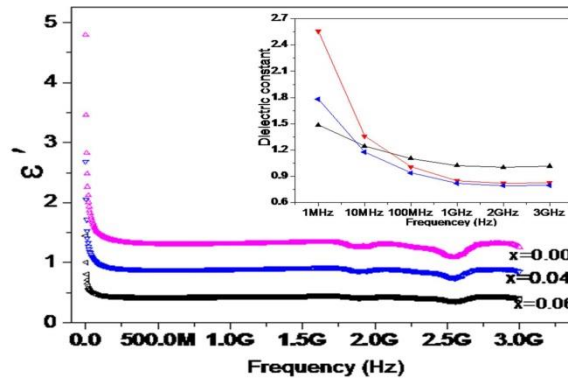


Fig. 8(a) Effect of variation on the dielectric constant versus frequency (b) the inset plot shows selective values of dielectric constant behavior versus frequency and Y³⁺ content (x)

3.5.2 Variation of dielectric loss tangent (tan δ) with frequency

Figure 9 shows the variation of dielectric loss (tanδ) with frequency and dielectric loss follows the trend of permittivity loss. Dielectric losses in ferrite system usually reflect in DC electrical resistivity. Therefore, the ferrites consisted of both the conducting as well as poorly conducting grain boundaries. Fig. 9 (inset) clearly showed that at high value of frequency, f > 1.5 GHz many resonance peaks were observed, which were the characteristics of dielectric loss tangent appeared due to un-damped dipoles [39]. The condition for observing a maximum in the dielectric losses of a dielectric material is given by:

$$\omega_{max}\tau = 1 \tag{12}$$

where, $\omega_{max} = 2\pi f_{max}$. Relaxation time(τ) is the jumping probability per unit time ‘p’ for the ionic/interfacial /electronic polarization and is written as

$$\tau = \frac{1}{2\pi f_{max}} = 2p (f_{max} \alpha p) \tag{13}$$

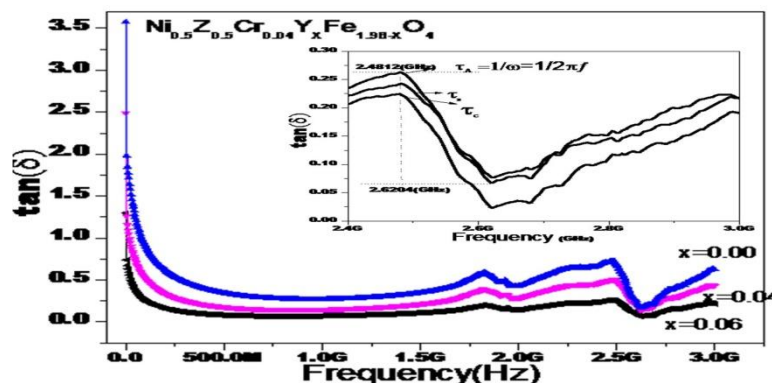


Fig.9 (a) Effect of variation on the dielectric loss tangent versus frequency (b) shows inset in the plot dielectric relaxation peaks with different Y³⁺ content.

The phenomenon of ferromagnetic resonance can be explained on the basis of the Debye relaxation process that occurs when the rate of hopping of electrons from Fe^{2+} to Fe^{3+} is nearly equal to the applied ac frequency.

3.5.3 AC-conductivity

The electrical conductivity in ferrite was mainly due to the hopping of electrons between the ions of the same element present in more than one valence state and distributed randomly over crystallographically equivalent sites. It can be observed from Fig.10 that as a normal behavior, σ_{ac} increased with frequency could be expressed at a constant temperature, as

$$\sigma_{ac} = \sigma_{dc}(T) + \sigma(\omega, T) \quad (14)$$

Where, (σ_{dc}) is dc conductivity. Moreover, it obeys a power law which could be written as

$$\sigma_{ac} = A\omega^n \quad (15)$$

Where A is temperature dependent constant parameter having units of conductivity (ohm.cm^{-1}) and ω is angular frequency. The exponent 'n' is a temperature dependent constant having value between 0 and 1 [40]. Fig.10 shows the variation of AC conductivity as a function of frequency. The trend attitude of AC conductivity showed a linear trend with increase of frequency. It was observed that for the electric field, the poorly conducting grain boundaries became more active at lower frequencies and hence long range inter-well hopping of electrons between Fe^{2+} and Fe^{3+} ions were less at lower frequencies for $x = 0.00$. As frequency of the applied field increases, the conductive grains promote the intra-well hopping of electron between Fe^{3+} and Fe^{2+} ions in the octahedral sites. Therefore we observed a gradual increase in ac conductivity with frequency. The frequency dependence can be explained with the help of Maxwell–Wagner two-layer model or the heterogeneous model of the polycrystalline structure of ferrites [43-44]. According to this theory two layers form dielectric structure. The first layer consisted of ferrite grains of fairly well conducting (Fe^{2+} ; ferrous ions), which was separated by a thin layer of poorly conducting substances, which forms the grain boundary. These grain boundaries were more active at lower frequencies; hence the hopping frequency of electron between Fe^{2+} and Fe^{3+} ions were less at lower frequencies. As the frequency of the applied field increased, the conductive grains became more active by promoting the hopping of electron between Fe^{2+} and Fe^{3+} ions, thereby increasing the hopping frequency. Thus we observed a gradual increase in conductivity with frequency.

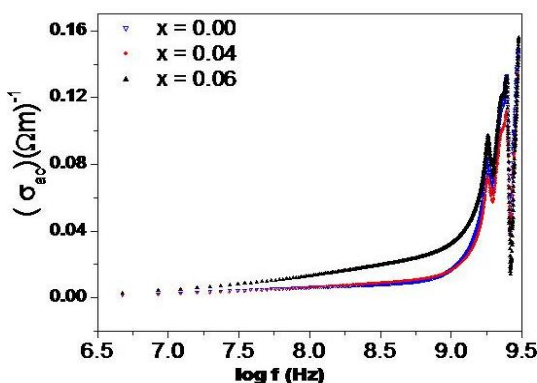


Fig. 10 AC conductivity as a function of frequency for Ni-Zn-Cr-Y-Fe spinel ferrites

Fig.11 shows the plot between $\log(\sigma)$ and $\log(\omega)$ in which ac conductivity increases with the increase of the applied field frequency. The increase in applied field frequency increases the hopping frequency between Fe^{2+} and Fe^{3+} and as a result the conductivity increases. In the present study, we have found that the reason for conduction in the synthesized samples were due to the

mechanism of hopping. The value of exponent 'n' varies between 0.48 and 0.59, which supported this finding.

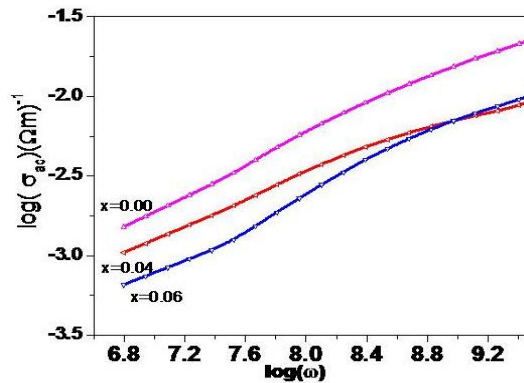


Fig. 11 Variation of $\log(\sigma_{ac})$ versus $\log(\omega)$ for Ni-Zn-Cr-Y-Fe spinel ferrites

3.5.4. Relationship between the dielectric constant and the resistivity

Fig.12 shows the relationship between the product values of dielectric constant and resistivity vs frequency from 1MHz to 3GHz.

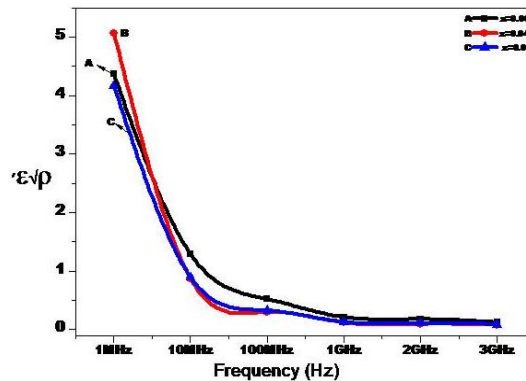


Fig.12 Relationship between $\epsilon'\sqrt{\rho}$ and frequency for Ni-Zn-Cr-Y-Fe spinel ferrites

The product of $\epsilon'\sqrt{\rho}$ decreased with the increase of applied frequency and became constant after 10 MHz.

4. Conclusions

The single phase spinel ferrites Ni-Zn-Cr-Y-Fe successfully synthesized using co-precipitation technique as confirmed by XRD analysis. The lattice constant lie in the range 8.354 - 8.430 Å and the average crystallite size calculated using Scherrer's formula lie in the range of 30.3 -106nm. The optical band gap of the prepared samples was obtained from UV-vis spectroscopy which revealed increase ($E_{dg} < E_{ig}$) with the increase of Y^{+3} ions content due to the formation of oxygen vacancies and the induction of lattice distortions, the electrical conductivity (σ) decrease. SEM analysis confirmed the morphology of the synthesized material. Yttrium Y^{3+} ions acted as grain growth inhibitor, which reduced the complex permeability. The variation of dielectric constant and loss tangent with frequency followed Maxwell-Wagner polarization model. The synthesized ferrites can be useful high frequencies microwave devices.

Acknowledgements

The author (Ghulam Mustafa) is thankful to Higher Education Commission (HEC) of Pakistan for providing financial support to carry out this work under IRSIP scholarship.

References

- [1] R. Tadi, K. Yong-II, A.K. Sarella, C.G. Kim, K.S. Ryu, J. Magn. Mater. **322**, 3372 (2010).
- [2] E. MelaGiriyappa, H.S. Jayanna, J. Alloys Compd., **482**,147 (2009).
- [3]E. Rezlescu, N. Rezlescu, C. Pasnicu, M. L. Craus, D. P. Popa, J. Magn. Mater. **117**,448 (1992) .
- [4] N. Rezlescu, L. Rezlescu, P. D. Popa, E. Rezlescu, J. Magn. Mater. **215- 216**,194 (2000).
- [5] M.B. Shelar, P. A. Jadhav, S. S. Chougule, M. M. Mallapur, B.K.Chougule, J. Alloys Compd. **476**,760 (2009).
- [6]S.M. Patange, S.E. Shirsath, B.G. Toksha, S.S. Jadhav, K.M. Jadhav,J.Appl. Phys. **06**, 023914 (2009).
- [7]T.J. Shinde, A.B. Gadkari, P.N.Vasambekar, J.Alloy.Comp.**513**,80 (2012).
- [8] M.Z. Said, Mater. Lett.**34**, 305 (1998)
- [9]Goran Stojanovic, Vladimir Srdic, and MarijaMaletin, Phys. stat. sol. (a) **205**,2464 (2008).
- [10] Kwang PyoChae, Young Bae Lee, Jae Gwang Lee, Sung Ho Lee,J. Magn. Mater. **220**, 59 (2000).
- [11] M.A. Ahmed, E. Ateia, S.I. El-Dek, Mater. Lett. **57**,4256 (2003).
- [12] M. Ishaque, M.U. Islama, M.A. Khan, I.Z. Rahman, A. Genson, S. Hampshire, Physica B **405**,1532 (2010).
- [13] K. Vijaya Kumar, A. Chandra Shekhar Reddy, D. Ravinder J. Magn. Mater., **263**,121 (2003).
- [14] A.D. Sheikh, V.L. Mathe, J. Mate. Sci.**43**,2018 (2008).
- [15] D.S. Mathew, R.S. Juang, J.Chem. Engg.**129**,51 (2007).
- [16] S. Dwevedi, K. K. Bharathi, G.Markandeyulu, IEEE Transactions on Magnetics **45**, 4253 (2009).
- [17]M.A. Ahmad, M.M. El-Sayed, M.M. El-Desoky, Physica B **405**,727 (2010).
- [18] M. Ishaque, M.U.Islam, Irshad Ali, M. Azhar Khan, I .Z. Rahman, Ceram.Inter. **38**,3337 (2012).
- [19] M.K. Shobana, Hoon Kwon, HeemanChoe, J. Magn. Mater. **324**,2245 (2012) .
- [20] B.D. Cullity, Second Edition Addison Wesley Publishing, Co;(1978) 42-46, 89, 92-102.
- [21] Ghulam Mustafa, M.U. Islam, Wenli Zhang, Yasir Jamil, Abdul Waheed Anwar, Mudassar Hussain, Mukhtar Ahmad, J. Alloys Comp, **618**, 428(2015).
- [22]I.H. Gul, A. Maqsooda, M. Naeem Ashiq, J. Alloy Compd. **507**,201 (2010).
- [23] Shahid Hussain, A. Maqsood, J. Magn. Mater. **316**,73 (2007).
- [24]Muhammad Naeem Ashiq, Muhammad Fahad Ehsan, Muhammad Javed Iqbal, Iftikhar Hussain Gul, J. Alloy.Comp. **509**, 5119 (2011) -5126.
- [25] W.D. Kingery, D.R. Uhlmann, Introduction to Ceramics, New York, Wiley, (1976).
- [26] P.A. Shaikh, R.C. Kambale, A.V. Rao, Y.D. Kolekar, J. Alloy.Comp. **492**, 590 (2010)
- [27]L. John Berchmans, R. KalaiSelvan, P.N. Selva Kumar, C.O. Augustin, J. Magn. Mater. **279**, (2004) 103-110.
- [28] S.C. Watawe, B.D. Sutar, B.D. Sarwade, B.K. Chougule, Int. J. Inorg. Mater.**3**,819 (2001)
- [29]S.A. Mazen, M.H. Abdallah, B.A. Sabrah, H.A.M. Hashem, Phys. Status. Solidi **134**,263 (1992).
- [30] William E. Lee, W. Mark Rainforth, Ceramic Microstructures: Property Control by Processing, Kluwer Academic Publishers, (1994).
- [31] E. Rezlescu, I. Sachelarie, P.D. Popa, N. Rezlescu, IEEE Trans. Magn. **36**,3962 (2000).
- [32]R.A. Smith, Semiconductors, Cambridge University Press, London, 2nd edn. (1978).

- [33] D.Ravinder, B.RaviKumar, Mater.Chem.and Physics **82**,321 (2003).
- [34] C.G. Koops, Phys. Rev. **38**,121 (1951).
- [35] N. Rezlescu, E. Rezlescu, C.Pasnicu, M.L.Craus, J.Phys.Condens.Matter, **6**, 5707 (1994).
- [36] Maxwell J.C., Vol. I,(Oxford university Press), Oxford section **328**, (1951).
- [37] A.S. Hudson, Marconi Rev. **37**,43 (1968).
- [38] A.M.Shaikh, S.S.Bellad, B.K.Chougule, J.Magn.Magn.Mater.**195**,384 (1999).
- [39] P.J Harrop, Dielectrics, London Butterworths, (1972).
- [40] K.L. Ngai, S.W.Martin, Phys. Rev. B **40**,10550 (1989).
- [41] M.A. El Hiti, J. Magn. Magn.Mater.**164**, 187 (1996).
- [42] J.A.D.Guillen, M.R.D.Gullen, K.P.Padmastree, A.F.Fuentes, J.Santamarfa, C.Leon, Solid State Ion, 179, (2008) 2160-2164.
- [43] Verma A, Thakur O P, Hsu J H, J. Alloys. Comp. **509**,5315 (2011) -5321.
- [44] I.G. Austin, N.F. Mott, Adv. Phys., **18**, 41 (1969).